Laser Induced Breakdown and Bubble Cavitation

[1]Giorgia Sinibaldi*; [2]Agostino Occhicone; [3]Francisco Alves Pereira; [1]Davide Caprini; [1]Luca Marino; [2]Francesco Michelotti; [1,4]Carlo Massimo Casciola

[1]*Department of Mechanical and Aerospace Engineering, La Sapienza, Rome, Italy;*
[2]*Department of Basic and Applied Sciences for Engineering, La Sapienza, Rome, Italy;*
[3]*Marine Technology Research Institute, CNR-INSEAN, Rome, Italy;*
[4]*CLNS@Sapienza, Istituto Italiano di Tecnologia, Rome, Italy*

Abstract

This work presents the results of an experimental investigation of laser induced cavitation. We find that the breakdown plasma can be randomly split in different branches depending on the laser energy and on the focusing angle. This behavior strongly affects the successive dynamics of the bubble and limits the reproducibility of the process. Using a custom fiber optic hydrophone, we correlate the elongated shape of the plasma with the number of shock waves detected at breakdown. The conditions for single breakdown shockwave emission and spherical expansion are thus identified, thus improving the reproducibly for laser-induced cavitation bubble.

Keywords: cavitation; laser induced bubble; fiber optic probe hydrophone

Introduction

Bubble cavitation is one of the most discussed topics in fluid dynamics. Generally, it is associated with erosion damage and high-frequency noise [1], but it is currently reconsidered for a wide range of modern applications within medicine [2], microfluidics [3] and other fields. The life of a cavitation bubble can be divided into four different phases: nucleation, growth, collapse and rebound. In this study, we focus on the bubble dynamics in pure water. In the context of the classical nucleation theory (CNT) [4], homogeneous nucleation is the condition where a single spherical bubble is formed in a volume of water due to energy fluctuations of the system. Laser-induced cavitation has been extensively used to create this condition experimentally as it allows the control of the breakdown position and a high reproducibility of the bubble dynamics, see e.g. Lauterborn (1972) [5], Vogel et al. (1996) [6], Philipp & Lauterborn (1998) [7], Vogel et al. (1999) [8], Ohl et al. (1999) [9], Vogel et al. (2005) [10], Lim et al (2010) [11], Obreschkow et al. (2013) [12], Tagawa et al. (2016) [13].

However, the characteristics of the setup such as focusing optics, laser energy and water quality can introduce deviations from the ideal single bubble condition. Here we report on the observation of multiple plasmas formation and analyze the effect of both the focusing angle and laser energy on the breakdown event and on the bubble growth. The pulsed laser beam is expanded, collimated and then focused by a parabolic mirror immersed in water to minimize spherical aberrations [12]. The characterisation of the phenomenon is done through the use of high-speed imaging and pressure measurements. In particular, a fiber optic hydrophone has been purposely developed to quantify the pressure peak of the shock waves emitted upon optical breakdown of the water medium and bubble collapse.

The first part of the study addresses the impact of the focusing optics on the bubble dynamics, specifically the effect of the converging angle and of the laser energy on the size and potential energy of the bubble. In a second part, we show how these two factors can affect the number and shape of plasmas, and consequently the pressure field.

Experimental setup

The setup consists of a stainless-steel chamber (120x120x120 mm^3) equipped with quartz windows for optical access (cavitation box in Fig. 1). Bubble generation is obtained by focusing a Q-switched Nd:YAG laser (Litron Nano S 35-15), which can deliver light pulses at the wavelength $\lambda = 532$ *nm*, with a duration of 8 *ns*, a maximum repetition rate of 15 *Hz* and a pulse energy up to 30 *mJ*. At the laser exit, 4% of the energy is extracted by a beam splitter and sent to a pyroelectric energy sensor in order to accurately measure the laser energy to be focused, see

*Corresponding Author, Giorgia Sinibaldi: giorgia.sinibaldi@uniroma1.it

Fig. 1. The beam, with energy E_L, then passes through a custom Galilean beam expander and is collimated to reach an off-axis parabolic aluminum mirror placed inside the cavitation box filled with pure water. The parabolic mirror was chosen to avoid spherical aberrations [12] and is off-axis to prevent laser beam back reflection into the laser source. Different beam expander magnifications (×8, ×6 and ×3) were tested to evaluate the effect of the focusing angle γ (53°, 33° and 17°, respectively).

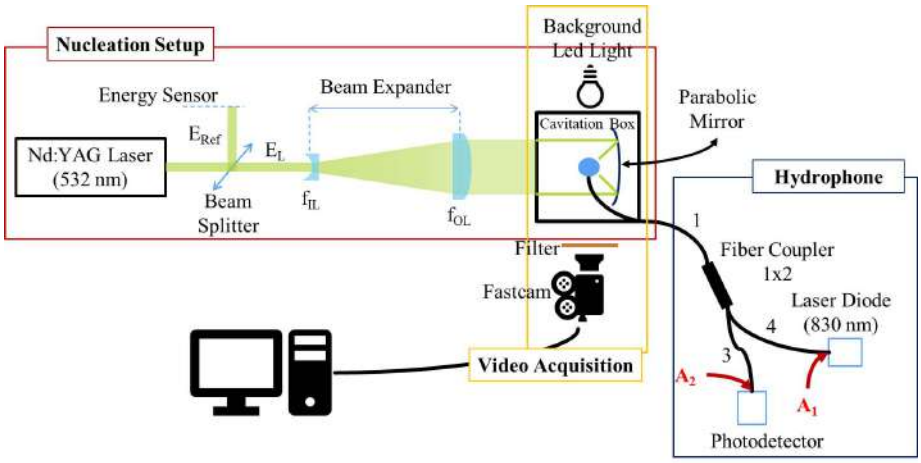

Fig. 1 Schematic of the experimental setup. System for bubble generation (red box), system for high speed acquisition (yellow box), custom fiber optic hydrophone setup (blue box).

High speed imaging is performed with a Photron Mini UX100 fast camera and a LED light for background illumination (see the yellow box in Fig. 1). The recordings are then analysed to investigate the bubble dynamics and the plasma characteristics.

A fiber optic probe hydrophone (FOPH) has been developed for local pressure measurements of the breakdown shock wave. The fiber optic allows to measure the refractive index change related to the density variation at shock wave passage. The FOPH setup is schematized in the blue box of Fig. 1. The light from a 1 *W* laser diode emitting at 830 *nm* is injected into a 2×1 fiber coupler (arm 4), and feeds an exit fiber that is immersed in water in the cavitation box and serves as the pressure probe (arm 1). This light reflects at the fiber-water interface back into the fiber coupler and is finally collected by an avalanche photodetector (arm 3). The output signal is acquired by a system with a bandwidth of 200 *MHz* and is recorded and analysed by a custom LabView software.

Results

In Fig. 2a, the values of the maximum bubble radius (R_{max}) measured with the fast camera are plotted as a function of the laser energy (E_L) for different focusing angles, 53° (black curve), 33° (red curve) and 17° (blue curve). The R_{max} values are the average over 64 consecutive events acquired at constant energy, and are plotted with their standard deviation. We used R_{max} to estimate the bubble potential energy as $E_B=\frac{4}{3}\pi(p_{amb}-p_v)R_{max}^3$, where p_{amb} is the ambient pressure, p_v is the vapor pressure (2.33 *kPa* in water at 20 *°C*). The E_B values are plotted in Fig. 2b together with the case of Vogel et al (1994) [14] for reference. The ratio between E_B and E_L represents the amount of laser energy converted into mechanical energy, ultimately responsible for shock wave emission and cavitation. Increasing the focusing angle, the conversion efficiency of our setup spans between 9% and 15%, while in the experiment of Vogel et al (1994) [14] a conversion efficiency of the 25% was obtained for ns-laser pulses. We note that the optical setups differ between the two experiments.

In Fig. 3 the experimental measurement of the temporal evolution of the bubble radius is shown. The effect of the focusing angle is shown in Fig. 3a for a fixed laser energy E_L = 26 *mJ*. Here, single bubble acquisitions at 160.000 *fps* are shown for each case. For greater focusing angles the first two rebounds are also shown. For the case at $\gamma\sim17°$ no clear rebound can be observed and data are therefore omitted in the plot. In Fig. 3b, the experimental

temporal evolution of the bubble radius is shown for high and low laser energy at a constant focusing angle γ~53°. A good agreement is found between the experimental data and the theoretical dependencies (solid line on the plot). The latter was obtained from the integration of the Keller-Miksis model [4, 15], a modified form of the Rayleigh-Plesset model.

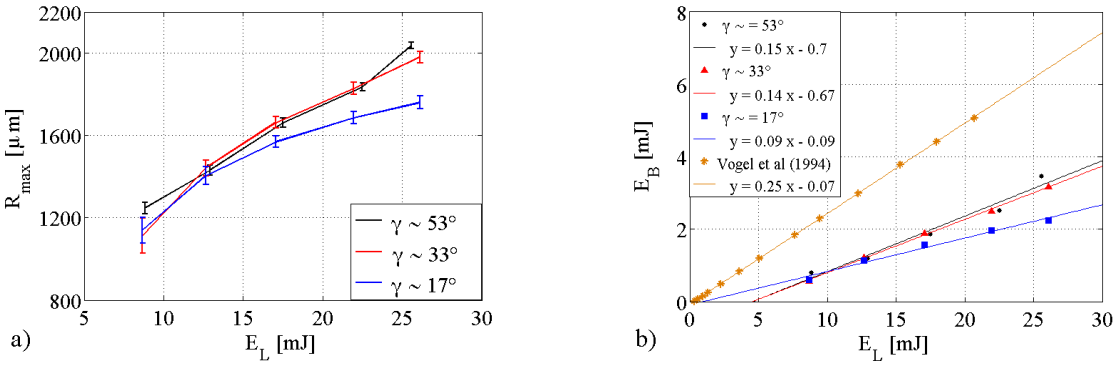

Fig. 2 Maximum bubble radius (a) and bubble potential energy (b) as a function of laser energy (bubble was imaged at 64.000 *fps*).

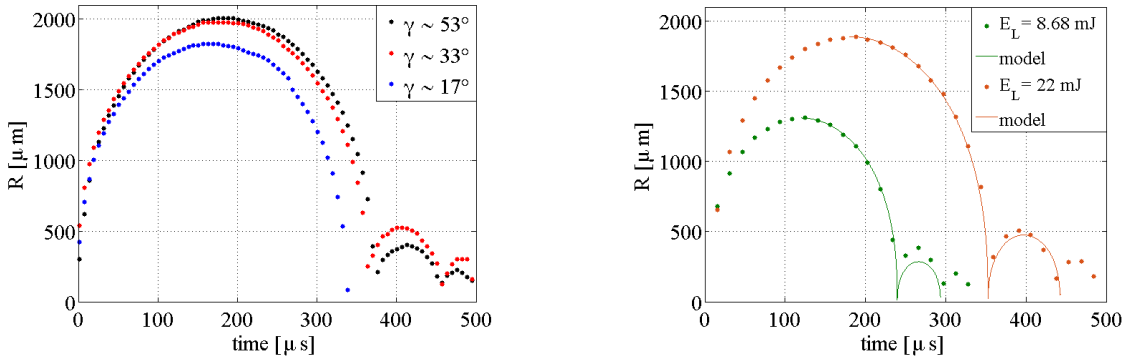

Fig. 3 Bubble radius evolution. (a) Effect of the focusing angle at E_L= 26 *mJ* (160000 *fps*). (b) Effect of the laser energy and comparison with the Keller-Miksis model at γ ~ 53° (64000 *fps*).

The dependency of the plasma shape on the main properties of the experimental set up has been already investigated, e.g. in [6, 13, 16, 17]. The main evidences are that the formation of multiple plasma depends on spherical aberrations, numerical aperture/focusing angle, liquid impurities and input laser energy. A small focusing angle favours the occurrence of multiple point-like plasmas. Moreover, multiple plasmas may be present even with "perfect" focusing, i.e. with no spherical aberrations. This is because the plasma occurs where the breakdown threshold is reached, which is not necessarily at the focusing point [13].

In Fig. 4a, we show the superposition of the images of the plasma (yellow) and of the bubble at its maximum expansion (red disk). The direction of the laser beam is marked by the green arrow. Such images were captured at 64000 *fps* for the different focusing angles and at a laser energy of 22 *mJ*. The change of the plasma length with the laser energy is shown in Fig. 4b for all focusing angles. From such figures it is evident that, at larger focusing angles, the plasma has a compact appearance and its length (see black curve) is almost constant with laser energy. Moreover, it is possible to appreciate from Fig. 4a that the plasma stretches with decreasing focusing angle, and is accompanied by a smaller bubble.

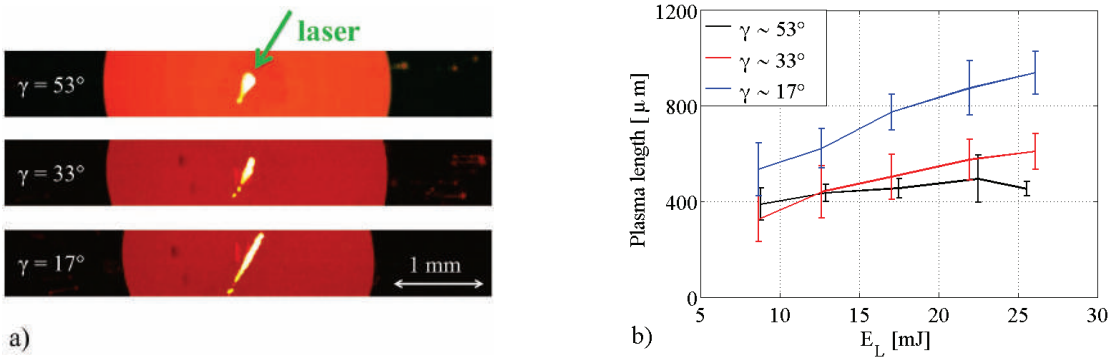

Fig. 4 Plasma morphology acquired at 64000 *fps*: a) superimposition of plasma (yellow) and bubble at maximum radius (red disk) at different focusing angles E_L = 22 *mJ*; b) plasma length as a function of the laser energy.

In Fig. 5 the grayscale intensity of the plasma (top frames) and the related intensity profile along the plasma axis (bottom) are shown. Each case is averaged over 64 bubble nucleation events. The averaging procedure permits to reject the random effect of the impurities and to obtain the deterministic influence of energy and focusing angle on the plasma shape. Two different focusing angles are reported, γ~17° (Fig. 5a) and γ~53° (Fig. 5b). As expected, by increasing the laser energy, the tip of the plasma remains fixed and the tail shifts backward in the direction of the light source [14, 16, 17]. Moreover, the region of highest intensity extends and the maximum intensity increases.

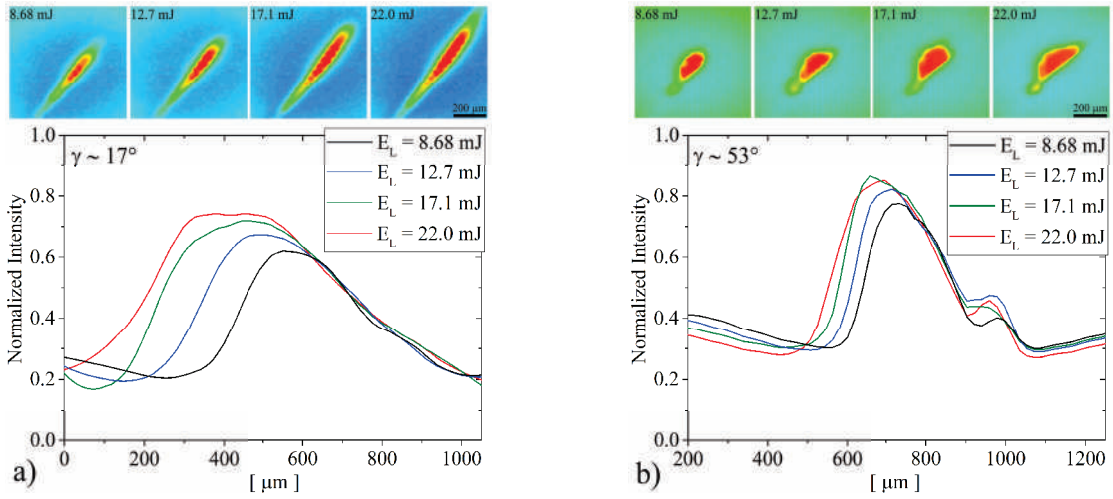

Fig. 5 Contour plot of the gray scale intensity of the plasma (top) and intensity profile along the plasma axis (bottom). a) γ ~ 17°, b) γ ~ 53°.

The main outcome of this analysis is the elongated shape of the plasma along the propagation direction of the laser beam. Considering that spherical aberrations have been substantially avoided by using the parabolic mirror, the plasma shape can depend only on the magnification parameters, i.e. the focusing angle, on the laser pulse energy and the random effects of the impurities in the liquid. Such elongation is the source of asymmetry of the breakdown shock wave, which can be detected from the pressure measurement obtained by placing the tip of the FOPH at different locations, defined with the angle θ of Fig. 6a [13]. We expect to measure a number of peaks equal to the number of shockwave fronts reaching the fiber optic. From the three graphs shown in Figs 6b, 6c and 6d, the anisotropy of the shockwave system is clear. In the case θ = 90° (Fig. 6b) a single peak for each focusing angle is present, thus indicating that only one shock wave is detected. In the cases θ = 45° (Fig. 6c) and θ = 0° (Fig. 6d) more than a peak is found, evidencing the existence of multiple shockwave fronts. It can be observed that, moving from 90° to 0°, the peak widen in time. The effect is more pronounced for a reduced focusing angle, in good agreement with the plasma shape observed in the video frames shown above (Fig. 4).

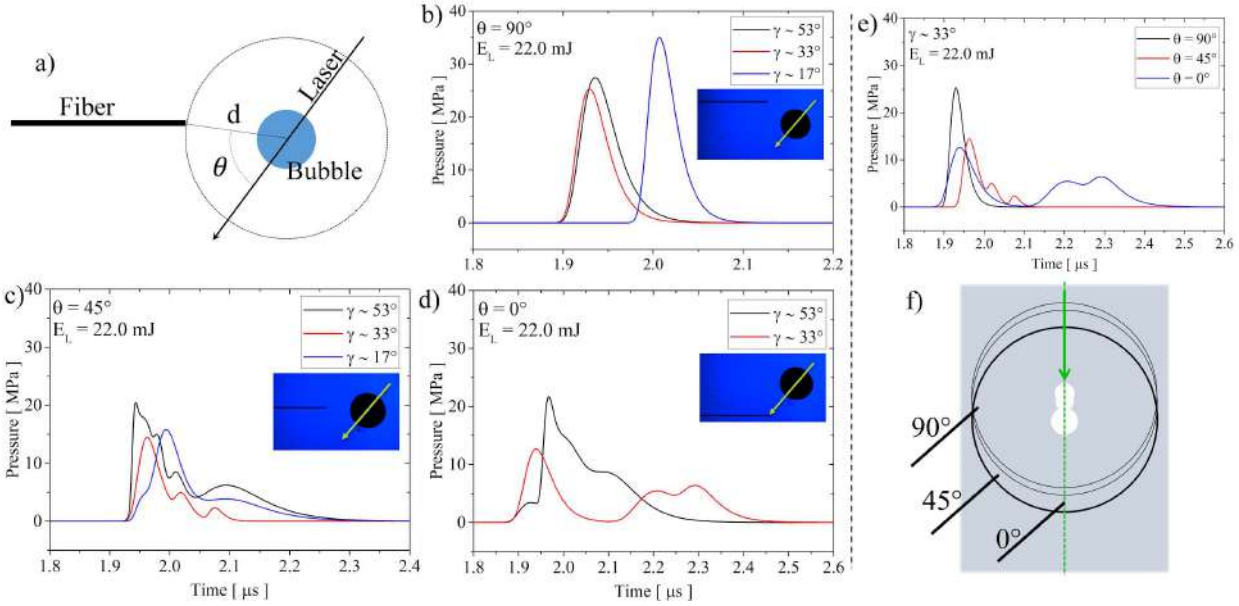

Fig. 6 Pressure signal at different probe locations as a function of focusing angle for a laser energy of 22 mJ: a) Sketch of the fiber position with respect to the laser direction; b) pressure signals at θ=90°; c) pressure signals at θ=45°; d) pressure signals at θ=0°; e) pressure signals for a focusing angle γ~33°; f) reconstruction of the wavefront system and the bubble initial configuration.

From the information collected with the hydrophone we can schematically reconstruct the multiple structure of the initial shock wave and the number of bubbles present in the first few nanoseconds. We assume that each shock wave is the superposition of different spherical components originating from different portions inside the plasma region [13]. An example of this reconstruction is shown in Figs 6e and 6f, related to the case which corresponds to $\gamma \sim 33°$ and $E_L = 22$ *mJ*. In Fig. 6e the number of shock waves reduces from three to one as the probe moves from $\theta = 0°$ to $\theta = 90°$, where the three pressure peaks reach the FOPH with the same delay and the overall shock wave appears as a single pressure pulse with the maximum amplitude, about 25 *MPa*. The schematic reconstruction gathered from this analysis is shown in Fig. 6f, with the three shockwaves and the subsequent bubble initial configuration.

Fig. 7 Superimposition of plasma (yellow), bubble at maximum radius (black disk) and maximum radius of the first rebound (small red disk). (a) $E_L = 26$ *mJ* , $\gamma \sim 53°$ and R_{max}=1970 *μm*. (b) $E_L =$ 9.5 *mJ* and $\gamma \sim 12°$ and $R_{max} \approx 550$ *μm*.

We found that almost all the investigated cases present an elongated plasma along the beam axis, a condition that leads to multiple shock waves emission, which in turn leads to multiple collapsing events with non-spherical bubbles at rebound, hence very poor reproducibility. However, we have identified two configurations that allow single spherical bubble nucleation with high repeatability as well as single rebound bubble after the first collapse: i) high energy and wide focusing angle; ii) low energy and narrow focusing angle. These two configurations are illustrated in Fig. 7a and 7b, respectively. Here, the superimposition of three frames for each case is reported: plasma (yellow), bubble maximum expansion (black disk) and the maximum expansion of the first rebound (small red disk). We note that in the first situation, the plasma has a conical form and remains located at the focusing point. In the second configuration, the plasma is instead point-like, however its location changes within the light cone, see the shifted position of the two bubbles in Fig. 7b.

Conclusion

In order to investigate laser-induced bubble cavitation in water, we assembled a laser nucleation set-up and combined high-speed visualizations with a fiber optic probe hydrophone (FOPH) to determine the pressure field induced during the process. A parabolic mirror immersed in water was used to minimize spherical aberrations [12]. However, multiple plasma sites were observed depending on the focusing angle and laser energy. To understand these effects, the characteristics of the laser-induced breakdown and bubble formation were first investigated for different laser beam convergence angles and different laser energies. The plasma length was found to increase with the laser energy, extending along the focusing cone towards the laser source. Shock pressure waves were measured with the FOPH in different positions with respect to the focusing location. We found that the laser-induced shock waves are in fact a collection of spherical shock waves emitted from the different plasma spots, demonstrating that multiple shock waves are directly related to the plasma shape. We found that single spherical bubbles could be produced with high reproducibility, at high energy and large focusing angle or at low energy and small focusing angle. However, we observed in this latter configuration that the bubble position in space could vary significantly because of the small energy density gradient along the focusing axis. In all other configurations, multiple breakdown sites and elongated plasmas are observed.

Future work will focus on the effect of ambient pressure on the bubble dynamics and on the interaction of the cavitation bubble with solid/membrane boundaries.

Acknowledgement

The research leading to these results has received funding from the European Research Council under the European Union's Seventh Framework Programme (FP7/2007-2013)/ERC Grant Agreement No. [339446].

References

[1] Plesset, M.S., Devine, R.E. (1966), *Effect of Exposure Time on Cavitation Damage*, Journal of Basic Engineering, 88(4).
[2] Brennen, C.E. (2015), *Cavitation in medicine*, Interface Focus, 5(5).
[3] Zwaan, E., Le Gac, S., Tsuji, K., Ohl, C.D. (2007), *Controlled Cavitation in Microfluidic Systems*, PRL, 98.
[4] F. Caupin and E. Herbert, "Cavitation in water," *C.R. Physique*, vol. 7, pp. 1000-1017, 2006.
[5] Lauterborn, W. (1972), *High-speed photography of laser-induced breakdown in liquids*, Applied Physics Letters, 21(1).
[6] Vogel, A., Busch, S., Parlitz, U. (1996), *Shock wave emission and cavitation bubble generation by picosecond and nanosecond optical breakdown in water*, The Journal of the Acoustical Society of America, 100(1).
[7] Philipp, A., Lauterborn, W. (1998), *Cavitation erosion by single laser-produced bubbles*, Journal of Fluid Mechanics, 361.
[8] Vogel, A., Noack, J., Nahen, K., Theisen, D., Busch, S., Parlitz, U., Hammer, D.X., Noojin, G.D., Rockwell B.A., Birngruber, R. (1999), *Energy balance of optical breakdown in water at nanosecond to femtosecond time scales*, Applied Physics B: Lasers and Optics, 68(2).
[9] Ohl, C.D., Kurz, T., Geisler, R., Lindau O., Lauterborn, W. (1999), *Bubble dynamics, shock waves and sonoluminescence*, Philosophical Transactions of the Royal Society of London A: Mathematical, 357(1751).
[10] Vogel, A., Noack, J., Huttman, G., and Paltauf, G. (2005), *Mechanisms of femtosecond laser nanosurgery of cells and tissues*, Applied Physics B, 81(8).
[11] Lim, K.Y., Quinto-Su, P.A., Klaseboer, E., Khoo, B.C., Venugopalan, V., Ohl, C.D. (2010), *Nonspherical laser-induced cavitation bubbles*, Physical Review E, 81(1).
[12] Obreschkow, D., Tinguely, M., Dorsaz, N., Kobel, P., de Bosset A., Farhat, M. (2013), *The quest for the most spherical bubble: experimental setup and data overview*, Experiments in Fluids, 54(5).
[13] Y. Tagawa, S. Yamamoto, K. Hayasaka and M. Kameda, "On pressure impulse of a laser-induced underwater shock wave," *J. Fluid Mech.*, vol. 8080, pp. 5-18, 2016.
[14] Vogel, A., Busch, S., Jungnickel, K., Birngruber, R. (1994), *Mechanisms of intraocular photodisruption with picosecond and nanosecond laser pulses*, Lasers in surgery and medicine, 15(1).
[15] J.B. Keller and M. Miksis, «Bubble oscillations of large amplitude,» *J. Acoust. Soc. Am.*, vol. 68, n. 2, pp. 628-633, 1980.
[16] Vogel, A., Nahen, K., Theisen, D., Noack, J. (1996), *Plasma formation in water by picosecond and nanosecond Nd: YAG laser pulses. I. Optical breakdown at threshold and superthreshold irradiance*, IEEE Journal of Selected Topics in Quantum Electronics, 2(4).
[17] Nahen, K., Vogel, A. (1996), *Plasma formation in water by picosecond and nanosecond Nd: YAG laser pulses. II. Transmission, scattering, and reflection*, IEEE Journal of Selected Topics in Quantum Electronics, 2(4).